J. Cent. South Univ. (2015) 22: 2586−2595
DOI: 10.1007/s11771-015-2788-z

Springer

Visual positioning of rectangular lead components based on Harris corners and Zernike moments

WANG Zu-jin(王祖进), HUANG Xiao-diao(黄筱调)

Department of Mechanical and Power Engineering, Nanjing Tech University, Nanjing 211816, China

Abstract: With the increasing necessities for reliable printed circuit board (PCB) product, there has been a considerable demand for high speed and high precision vision positioning system. To locate a rectangular lead component with high accuracy and reliability, a new visual positioning method was introduced. Considering the limitations of Ghosal sub-pixel edge detection algorithm, an improved algorithm was proposed, in which Harris corner features were used to coarsely detect the edge points and Zernike moments were adopted to accurately detect the edge points. Besides, two formulas were developed to determine the edge intersections whose sub-pixel coordinates were calculated with bilinear interpolation and conjugate gradient method. The last experimental results show that the proposed method can detect the deflection and offset, and the detection errors are less than 0.04° and 0.02 pixels.

Key words: visual positioning; Harris corners; Zernike moments; edge detection; sub-pixel; image registration

1 Introduction

With the smaller size of chip components and the greater number of leads, there has been a considerable demand for the placement machine with higher positioning accuracy. So, a faster and more accurate positioning algorithm is needed. The positioning algorithms of placement machine vision system mainly include the positioning of chip components and printed circuit boards (PCBs). In the process of positioning for chip components, the offset and deflection are detected. The offset is the distance from the center of a chip component to the center of a nozzle, and the deflection is the angle between a chip component and the placement position on a PCB board. In the process of positioning for PCB boards [1], the positioning mark on the mother board is detected to obtain the conversion relationship between the coordinate system of a PCB board and the coordinate system of a placement machine. Some scholars have studied the related algorithms of placement machine vision system [2−5]. Through the analysis to the work of previous studies, we can find that the existing methods detect the offset and deflection separately, and do not put them together into consideration.

Commonly used edge detection operators include Sobel, Robert, Canny, and LOG, and so on, whose positioning accuracy can only reach one pixel and can not meet the accuracy requirements of the placement machine vision system. Therefore, a sub-pixel edge detection algorithm is needed to improve the positioning accuracy of components. The edge detection model of the sub-pixel edge detection method is different from the models of the other pixel edge detection operators such as Sobel, Robert, Canny and LOG operators. LYVERS et al [6] used spatial moments to detect the sub-pixel edges of an image, and six spatial moments were used to calculate the four parameters of the edge model, but spatial moments were not orthogonal. So, this method had redundant information, and the calculation amount is large. GHOSAL and MEHROTRA [7] used Zernike orthogonal moments to detect the sub-pixel edges, and three Zernike moments were used to calculate the four parameters of an ideal edge model, but this method also had some limitations, such as the lower positioning accuracy and the larger errors at the neighborhood of the edge intersections. For the limitations of Ghosal method, GAO et al [8] proposed an improved algorithm, but this method also did not consider the larger errors at the neighborhood of the edge intersections.

In this work, a new detection method was proposed, and a rectangular lead component was taken as the research object. First, the connected regions of leads were labeled and the second central moments were calculated to determine the lead shape of the component.

Foundation item: Project(51175242) supported by the National Natural Science Foundation of China; Project(BA2012031) supported by the Jiangsu Province Science and Technology Foundation of China
Received date: 2014−05−27; **Accepted date:** 2014−10−20
Corresponding author: HUANG Xiao-diao, Professor; Tel: +86−15951675754; E-mail: njgdhxd1@126.com

Then, the Harris corner features were extracted to coarsely detect the edge points. Next, five 7×7 templates were used to calculate the Zernike moments to accurately detect the edge points. In addition, two formulas were developed to determine the edge intersections. Bilinear interpolation and conjugate gradient method were used to calculate the sub-pixel coordinates of the edge intersections. Then, the edge points were classified and fitted a straight line to obtain the deflection, and the registration of two images was completed to obtain the offset. Finally, three experiments were designed and the experimental results show that the positioning accuracy of the general edge points and edge intersections is much higher compared with Ghosal algorithm, and the detection accuracy of the offset and deflection is much higher than that of Harris or Harris-Ghosal algorithm.

2 Image preprocessing

The component lead images collected with the placement machine vision system have some dim details [9] which make many leads break into two connected regions. So, it is necessary to preprocess the component image. The main steps are as follows:

1) Process the image by using grayscale morphological closing operation with a 3×3 structuring element to filter out the noises and brighten the dim details;

2) Convert the image into a binary image with the automatic threshold method;

3) Process the image by using binary morphological opening operation with a 2×2 structuring element to remove the burrs points on the edges of leads.

The four connected neighborhoods of a burrs point only have a bright point. Image preprocessing results are shown in Fig. 1.

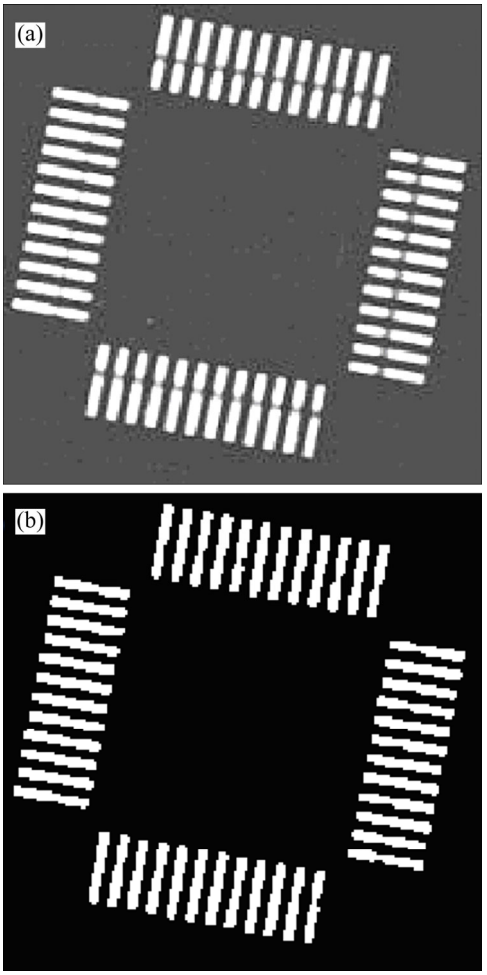

Fig. 1 Image preprocessing: (a) Original grayscale image; (b) Preprocessed image

3 Discrimination of lead shape

According to the shape of leads, chip components can be divided into rectangular lead components and round lead components. For different shapes of leads, the corresponding positioning algorithms are also different. So, the shape of leads needs to be determined before positioning a chip component. First, the connected region of each lead is labeled [10−12]. Then, two second-order central moments of the labeled lead are calculated. If the ratio of two central moments is much larger than one, the shape of leads is rectangular. If the ratio is approximately equal to one, the shape is round.

3.1 Labeling of connected regions

The connected region of each lead is labeled with morphological dilation operation. As the width of gap between two connected regions is at least one pixel, so using a 3×3 structural element can ensure that each dilation operation will not produce points within the other connected regions, and then the dilated image is intersected with the original image, thus the dilation will be limited within the connected region. Specific steps are as follows:

1) Randomly select a bright point B_0 from a connected region of the original image I.

2) Process the image by using the dilate operation with a 3×3 structuring element S_0, and intersect the dilated image with the original image to get B_1. Repeat the dilation and intersection operation until B_{i+1} is equal to B_i to label a connected region. The algorithm is summarized as

$$B_{i+1} = (B_i \oplus S_0) \cap I \quad (1)$$

3) Delete the connected region from the original image.

4) Repeat the above steps until the original image has no bright point. So far, all of the connected regions are labeled.

3.2 Calculations of second central moments

Let $f(i, j)$ be a digital image of $M\times N$, then the $(p+q)$-th order geometric moment m_{pq} and $(p+q)$-th order central moment μ_{pq} can be calculated by

$$m_{pq}=\sum_{i=1}^{M}\sum_{j=1}^{N} i^p j^q f(i,j) \tag{2}$$

$$\mu_{pq}=\sum_{i=1}^{M}\sum_{j=1}^{N} (i-i_0)^p (j-j_0)^q f(i,j) \tag{3}$$

where $i_0=m_{10}/m_{00}$, $j_0=m_{01}/m_{00}$, $p, q\in[0,1,2,\ldots]$.

Assume that $\boldsymbol{X}$ is the horizontal coordinate matrix of a labeled region, $\boldsymbol{Y}$ is the vertical coordinate matrix, and their size is $n\times1$. The second central moments of the labeled region are calculated as follows.

$$m_{00}=\sum_{(x,y)\in S} f(x,y)=n \tag{4}$$

$$m_{10}=\sum_{(x,y)\in S} x\cdot f(x,y)=\sum_{i=1}^{n}\boldsymbol{X}(i) \tag{5}$$

$$m_{01}=\sum_{(x,y)\in S} y\cdot f(x,y)=\sum_{i=1}^{n}\boldsymbol{Y}(i) \tag{6}$$

$$m_{20}=\sum_{(x,y)\in S} x^2\cdot f(x,y)=\sum_{i=1}^{n}\boldsymbol{X}^2(i) \tag{7}$$

$$m_{02}=\sum_{(x,y)\in S} y^2\cdot f(x,y)=\sum_{i=1}^{n}\boldsymbol{Y}^2(i) \tag{8}$$

$$\mu_{02}=m_{02}-m_{01}^2/m_{00} \tag{9}$$

$$\mu_{20}=m_{20}-m_{10}^2/m_{00} \tag{10}$$

Table 1 lists the moment features of some leads, where R_o represents a round component and R_e represents a rectangle component.

4 Extractions of Harris corner features

One corner of an image is the intersection point of two edges, and has rotation invariance and translational invariance. Harris operator [13−14] is an effective extraction operator of corner features. The computation process is simple, and the extracted feature points are uniform. So, we take Harris corner as the positioning features of rectangular lead components. The extraction steps of Harris corner features are as follows.

1) Calculate the gradients I_x and I_y of the image $I(x, y)$ in the x and y directions:

$$\begin{cases} I_x=\dfrac{\partial I}{\partial x}=I\otimes f_x \\ I_y=\dfrac{\partial I}{\partial y}=I\otimes f_y \end{cases} \tag{11}$$

where f_x=[−1 0 1; −1 0 1; −1 0 1], f_y=[−1 −1 −1; 0 0 0; 1 1 1], and $\otimes$ is the convolution operation.

2) Calculate the products of the gradients:

$$\begin{cases} I_x^2=I_x\cdot I_x \\ I_y^2=I_y\cdot I_y \\ I_{xy}=I_x\cdot I_y \end{cases} \tag{12}$$

3) Weight the products with a Gaussian function:

$$\begin{cases} A=I_x^2\otimes w \\ B=I_y^2\otimes w \\ C=I_{xy}\otimes w \end{cases} \tag{13}$$

where w is a 9×9 Gaussian window function.

4) Calculate the determinant and trace of the autocorrelation matrix $\boldsymbol{M}$:

$$\begin{cases} \det\boldsymbol{M}=\boldsymbol{AC}-\boldsymbol{B}^2 \\ \text{trace}\,\boldsymbol{M}=\boldsymbol{A}+\boldsymbol{C} \end{cases} \tag{14}$$

5) Calculate the response value R of each corner point, and if the value is less than a threshold t, R is set to zero:

$$R=\det\boldsymbol{M}-\alpha(\text{tr}\,\boldsymbol{M})^2 \tag{15}$$

where α is an empirical constant and its value is 0.04.

6) Remove the non-maxima points in the 3×3 neighborhoods. The rest maxima points are the corners of the image.

5 Zernike moments and sub-pixel edge detection

5.1 Definition of Zernike moments

The $(n+m)$-th order Zernike moment of a two-dimensional function $f(x, y)$ is defined as [15]

$$Z_{nm}=\frac{n+1}{\pi}\iint R_{nm}(\rho)\mathrm{e}^{\mathrm{j}m\theta}f(\rho,\theta)\mathrm{d}\rho\mathrm{d}\theta \tag{16}$$

where n is a non-negative integer, $n-|m|$ is an even and

Table 1 Moment features of some leads

Lead No.	Lead shape	m_{00}	m_{01}	m_{10}	m_{02}	m_{20}	μ_{02}	μ_{20}	μ_{20}/μ_{02}
1	R_o	64	11863	4793	2199225	359299	306.7	348.2	1.1
2	R_o	63	13069	4720	2711371	353982	279.6	356.6	1.3
3	R_e	113	10015	2806	887999	77466	386.4	7787.8	20.2
4	R_e	109	11268	2397	1165198	60017	355.6	7305.0	20.5

$n \geq |m|$, j is the imaginary unit, and the radial polynomial R_{nm} can be expressed as

$$R_{nm}(\rho) = \sum_{s=0}^{(n-|m|)/2} \frac{(-1)^s[(n-s)!]\rho^{n-2s}}{s!(\frac{n+|m|}{2}-s)!(\frac{n-|m|}{2}-s)!} \tag{17}$$

5.2 Principle of Ghosal algorithm

Ghosal uses a two-level ideal edge model [16−17] to detect the sub-pixel edges, and the model is shown in Fig. 2. The circle is a unit circle, L is the ideal edge of the image, h is the gray of the background, k is the step gray, l is the distance from the origin point to the ideal edge, and φ is the angle between the x-axis and l. Figure 2(a) is rotated clockwise with angle φ to obtain Fig. 2(b). The edge is parallel to the y-axis in Fig. 2(b), so we can get

$$\iint_{x^2+y^2 \leq 1} f'(x,y)y\mathrm{d}x\mathrm{d}y = 0 \tag{18}$$

where $f'(x, y)$ is the edge function of the rotated edge.

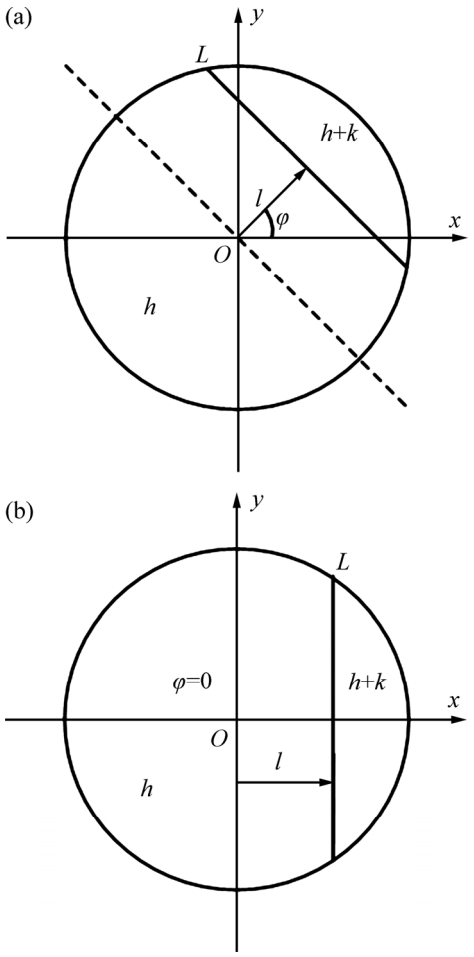

Fig. 2 Two-level ideal edge model: (a) Original edge model; (b) Rotated edge model

Zernike moments before and after rotation satisfy the following relationship:

$$Z'_{nm} = Z_{nm}\mathrm{e}^{-\mathrm{j}m\varphi} \tag{19}$$

From Eq. (19), we can get that Zernike moments have the character of rotation invariance, namely, the amplitude is constant, and only the phase angle can change. With this feature of Zernike moments, the ideal edge model is rotated to calculate the four edge parameters.

By Eq. (18), we can get that the imaginary part of the 2nd order Zernike moment of the rotated image is zero.

$$\mathrm{Im}[Z'_{11}] = \sin\varphi\,\mathrm{Re}[Z_{11}] - \cos\varphi\,\mathrm{Im}[Z_{11}] = 0 \tag{20}$$

where $\mathrm{Im}[Z_{11}]$ is the imaginary part of Z_{11}, and $\mathrm{Re}[Z_{11}]$ is the real part of Z_{11}.

So, the rotation angle φ of the edge can be calculated by

$$\varphi = \arctan\left(\frac{\mathrm{Im}[Z_{11}]}{\mathrm{Re}[Z_{11}]}\right) \tag{21}$$

The three integral kernel functions of Zernike moments are

$$\begin{cases} V_{00} = 1 \\ V_{11} = x - \mathrm{j}y \\ V_{20} = 2x^2 + 2y^2 - 1 \end{cases} \tag{22}$$

So, three Zernike moments can be calculated.

$$\begin{aligned} Z'_{00} &= \int_{-1}^{l}\int_{-\sqrt{1-x^2}}^{\sqrt{1-x^2}} hV_{00}\mathrm{d}y\mathrm{d}x + \int_{l}^{1}\int_{-\sqrt{1-x^2}}^{\sqrt{1-x^2}} (h+k)V_{00}\mathrm{d}y\mathrm{d}x \\ &= h\pi + \frac{k\pi}{2} - k\sin^{-1}(l) - kl\sqrt{1-l^2} \end{aligned} \tag{23}$$

$$\begin{aligned} Z'_{11} &= \int_{-1}^{l}\int_{-\sqrt{1-x^2}}^{\sqrt{1-x^2}} hV_{11}\mathrm{d}y\mathrm{d}x + \int_{l}^{1}\int_{-\sqrt{1-x^2}}^{\sqrt{1-x^2}} (h+k)V_{11}\mathrm{d}y\mathrm{d}x \\ &= \frac{2k(1-l^2)^{3/2}}{3} \end{aligned} \tag{24}$$

$$\begin{aligned} Z'_{20} &= \int_{-1}^{l}\int_{-\sqrt{1-x^2}}^{\sqrt{1-x^2}} hV_{20}\mathrm{d}y\mathrm{d}x + \int_{l}^{1}\int_{-\sqrt{1-x^2}}^{\sqrt{1-x^2}} (h+k)V_{20}\mathrm{d}y\mathrm{d}x \\ &= \frac{2kl(1-l^2)^{3/2}}{3} \end{aligned} \tag{25}$$

By Eqs. (23)−(25), l is calculated.

$$l = \frac{Z'_{20}}{Z'_{11}} \tag{26}$$

Then, the sub-pixel coordinates of the edge points can be calculated by

$$\begin{bmatrix} x_s \\ y_s \end{bmatrix} = \begin{bmatrix} x \\ y \end{bmatrix} + l\begin{bmatrix} \cos(\varphi) \\ \sin(\varphi) \end{bmatrix} \tag{27}$$

where (x_s, y_s) is the sub-pixel coordinate of an edge point, and (x, y) is the pixel coordinate of the edge point.

5.3 Principle of improved algorithm

The edge model of the sub-pixel edge detection used in this work is shown in Fig. 3. The circle is a unit circle, L is the ideal edge of the image, ab and cd are the image edges in different order Zernike moments conditions, h is the gray of the background, k is the step gray, l is the distance from the origin point to the ideal edge, l_1 and l_2 are the distances from the origin point to the edge ab and cd, and φ is the angle between the x-axis and l. Figure 3(a) is rotated clockwise with angle φ to obtain Fig. 3(b).

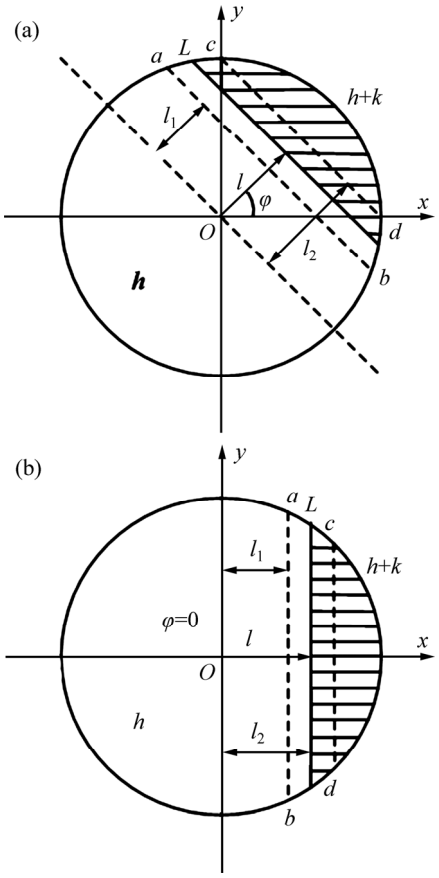

Fig. 3 Model of sub-pixel edge detection: (a) Original edge model; (b) Rotated edge model

Ghosal only uses three Zernike moments calculated with three 5×5 templates to detect the edge points, and the edge detection accuracy is low. So, we calculate five Zernike moments with five 7×7 templates to detect the edge points. Another two Zernike moments are calculated in the following manner.

$$Z'_{31}=\int_{-1}^{l}\int_{-\sqrt{1-x^2}}^{\sqrt{1-x^2}}hV_{31}\mathrm{d}y\mathrm{d}x+\int_{l}^{1}\int_{-\sqrt{1-x^2}}^{\sqrt{1-x^2}}(h+k)V_{31}\mathrm{d}y\mathrm{d}x$$
$$=k[\frac{4}{5}l^2(1-l^2)^{3/2}-\frac{2}{15}(1-l^2)^{3/2}] \tag{28}$$

$$Z'_{40}=\int_{-1}^{l}\int_{-\sqrt{1-x^2}}^{\sqrt{1-x^2}}hV_{40}\mathrm{d}y\mathrm{d}x+\int_{l}^{1}\int_{-\sqrt{1-x^2}}^{\sqrt{1-x^2}}(h+k)V_{40}\mathrm{d}y\mathrm{d}x$$
$$=k[-\frac{2}{5}l(1-l^2)^{3/2}+\frac{16}{15}l^3(1-l^2)^{3/2}] \tag{29}$$

where the two integral kernel functions are

$$\begin{cases}V_{31}=(3x^3+3xy^2-2x)+j(3y^3+3x^2y-2y)\\ V_{40}=6(x^4+y^4)+12x^2y^2-6(x^2+y^2)+1\end{cases} \tag{30}$$

The edge model at the intersections is shown in Fig. 4. The circle is a unit circle, h is the gray of the background, k is the step gray, φ is the angle between the x-axis and the bisector of the edge angle, and α is the angle between the edge and the bisector. Figure 4(a) is rotated clockwise with angle φ to obtain Fig. 4(b).

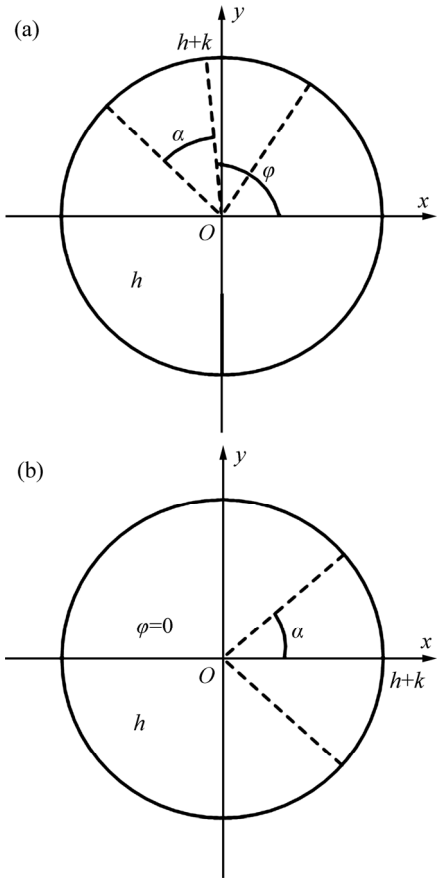

Fig. 4 Edge model at intersections: (a) Original edge model; (b) Rotated edge model

The rotated Zernike moments are calculated.

$$Z'_{pq}=\int_0^{2\pi}\int_0^1 hV_{pq}(\rho,\psi)\rho\mathrm{d}\rho\mathrm{d}\psi+$$
$$\int_{-\theta}^{\theta}\int_0^1(h+k)V_{pq}(\rho,\psi)\rho\mathrm{d}\rho\mathrm{d}\psi \tag{31}$$

Substituting $x=\rho\cos\psi$ and $y=\rho\sin\psi$ into Eqs. (22) and (30), $V_{pq}(\rho, \psi)$ can be obtained.

By Eq. (31), the following equation is obtained.

$$\begin{cases}Z'_{00}=h\pi+(k+h)\theta\\ Z'_{11}=\dfrac{2}{3}(k+h)\sin\theta\\ Z'_{20}=0\\ Z'_{31}=-\dfrac{2}{15}(k+h)\sin\theta\\ Z'_{40}=h\pi+(k+h)\theta\end{cases} \tag{32}$$

At the intersections, five Zernike moments satisfy the following relationship.

$$3Z'_{11}+15Z'_{31}=0 \tag{33}$$

$$Z'_{00}-Z'_{40}=0 \tag{34}$$

At the general edge points, the following equations are obtained.

$$3Z'_{11}+15Z'_{31}=12kl^2\sqrt{(1-l^2)^3} \tag{35}$$

$$Z'_{00}-Z'_{40}=h\pi+\frac{k\pi}{2}-k\sin^{-1}(l)-kl\sqrt{1-l^2}-k[-\frac{2}{5}l(1-l^2)^{3/2}+\frac{16}{15}l^3(1-l^2)^{3/2}] \tag{36}$$

So, we can get two formulas to determine the edge intersections.

$$\eta=3Z'_{11}+15Z'_{31} \tag{37}$$

$$\varepsilon=Z'_{00}-Z'_{40} \tag{38}$$

Select two appropriate thresholds T_1 and T_2. If $|\eta| \leq T_1 \cap |\varepsilon| \leq T_2$, the edge point is an intersection; else, the edge point is a general point.

When an edge intersection is found, we need to use relevant criteria to accurately calculate the sub-pixel coordinates of the intersection. Bilinear interpolation method is used to get the sub-pixel gray between the pixel points, and conjugate gradient method [18−19] is used to optimize the sub-pixel coordinates of the intersection. Conjugate gradient method only uses the first order derivative information and requires a small amount of storage, so it has good convergence and high stability and does not need any external parameters. The expression of the objective function is

$$\begin{cases} x'=x+\eta(x,y)/d_{\eta x}(x,y)+\varepsilon(x,y)/d_{\varepsilon x}(x,y) \\ y'=y+\eta(x,y)/d_{\eta y}(x,y)+\varepsilon(x,y)/d_{\varepsilon y}(x,y) \end{cases} \tag{39}$$

where the initial value of (x, y) is the intersection; $d_{\eta x}(x, y)$ and $d_{\eta y}(x, y)$ are the first order partial derivatives of the function $\eta(x, y)$; $d_{\varepsilon x}(x, y)$ and $d_{\varepsilon y}(x, y)$ are the first order partial derivatives of the function $\varepsilon(x, y)$. After several iterations, the sub-pixel coordinates of the intersection can be obtained.

6 Visual positioning

6.1 Detection of deflection angle

The main steps of detection are as follows:

1) Delete the false corner points. The discrimination method of the edge intersections is used to distinguish the false corner points.

2) Mark each corner in the x−y coordinate system.

3) Find the corner with the smallest x-coordinate. Delete this corner from the corner set.

4) Repeat step 3) twice to obtain the coordinates of another two corners.

5) Fit a straight line for the three points with the least square method and calculate the distances from the remaining corners to the straight line to find the rest corners belonging to the same class. Similarly, classify the other corners at the outermost side.

6) Fit a straight line for the four classes of corners with the least square method. Remove the classified corners.

7) Classify and fit the remaining corners.

8) Calculate the average value of the slopes of eight straight lines to get the deflection angle θ.

One of the classification results is shown in Fig. 5.

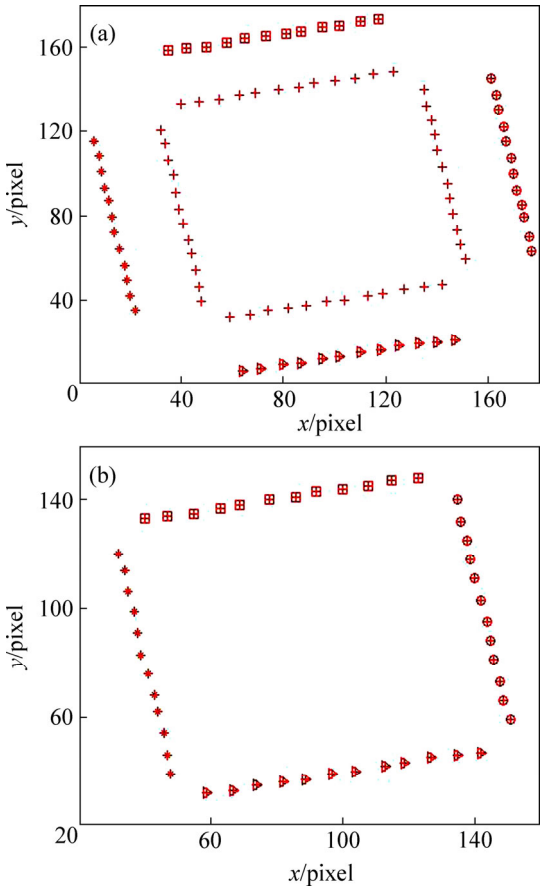

Fig. 5 Classification results: (a) Classification of corners at outermost side; (b) Classification of corners at innermost side

6.2 Detection of offset

Commonly used image registration methods include grayscale-based registration and feature-based registration [20−21]. The former is sensitive to the grayscale changes, rotation, deformation and block, and its computational complexity is high. The latter can overcome the disadvantages of the former, and has been widely used in image registration fields [22−24]. Feature points are much less than pixel points in an image, thus the amount of calculation is greatly reduced in the matching process. The registration of feature points is sensitive to the

changes of position, so the registration accuracy is high. So, we choose the image registration method based on Harris corners to detect the offset of chip components.

The main steps of image registration are as follows.

1) Rotate the image with the bicubic interpolation method. The rotation angle is θ.

2) Take the eight pixels near a corner as a feature point vector;

3) Match the feature point vectors of the rotated image and the standard image to get the two best matching points. The standard images are stored in the placement machine vision system and have no deflection and offset.

4) Calculate the coordinate differences between the two matching points to obtain the offset.

One of the registration results is shown in Fig. 6.

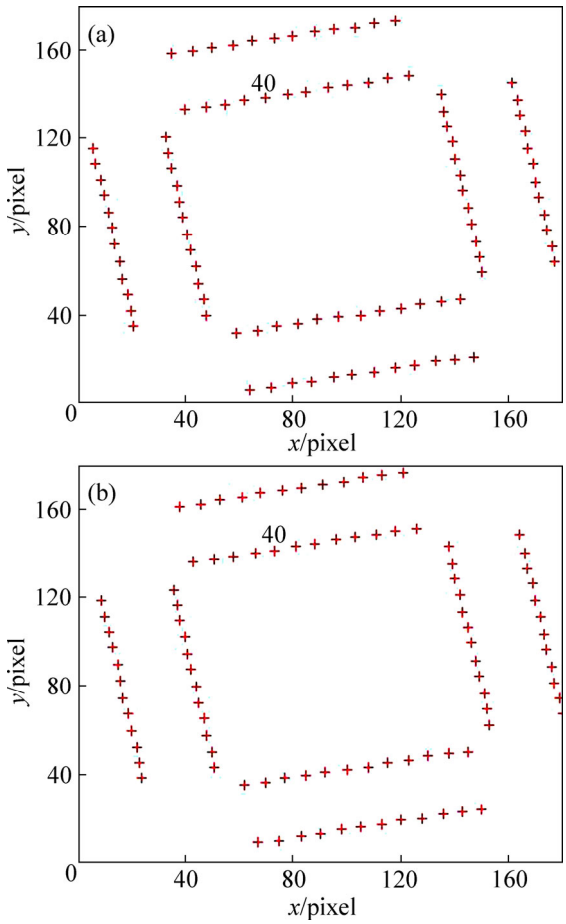

Fig. 6 Results of image registration: (a) Original image; (b) Offset image

7 Improved algorithm formulations

For the limitations of Ghosal algorithm, we present an improved algorithm. The specific steps of the improved algorithm are as follows.

1) Use Harris corners operator to detect the pixel edge points.

2) Calculate the 7×7 templates (M_{00}, M_{11}, M_{20}, M_{31} and M_{40}), and the calculation method has been shown in Ref. [25].

3) Use the templates to calculate the five Zernike moments (Z_{00}, Z_{11}, Z_{20}, Z_{31} and Z_{40}) of each edge point.

4) Determine whether the sub-pixel edge point is near an edge intersection.

5) Classify and fit the coordinates of the sub-pixel edge points with the least squares method to get the deflection angle.

6) Match the feature point vectors of the two images to get the offset.

8 Experiments and results analysis

In order to validate the effectiveness and superiority of the improved algorithm, three experiments are designed.

The test image of the first experiment is shown in Fig. 7. The image has been processed by the edge smoothing to simulate the actual image. The detection results are listed in Tables 2 to 5, in which the last row is the mean of the positioning error's absolute. From the detection results, the positioning accuracy of the improved method is much higher than Ghosal method for the edge points of the various edges.

Fig. 7 Test image

Table 2 Hypotenuse sub-pixel coordinates detection

Edge point	Ghosal	Improved algorithm
(312,98)	(311.8255,98.1813)	(311.9772,98.0332)
(311,99)	(310.8249,99.1746)	(310.9779,99.0218)
(310,100)	(309.8197,100.1787)	(309.9770,100.0217)
(309,101)	(308.8218,101.1780)	(308.9780,101.0224)
(308,102)	(307.8245,102.1750)	(307.9778,102.0223)
(307,103)	(306.8251,103.1734)	(306.9775,103.0230)
(306,104)	(305.8249,104.1719)	(305.9784,104.0204)
(305,105)	(304.8204,105.1797)	(304.9772,105.0218)
Mean error	0.1767, 0.1766	0.0224, 0.0233

Table 3 Horizontal edge sub-pixel coordinates detection

Edge point	Ghosal	Improved algorithm
(135,292)	(135,292.1283)	(135,292.0622)
(136,292)	(136,292.1283)	(136,292.0622)
(137,292)	(137,292.1283)	(137,292.0622)
(138,292)	(138,292.1283)	(138,292.0622)
(139,292)	(139,292.1283)	(139, 292.0622)
(140,292)	(140,292.1283)	(140, 292.0622)
(141,292)	(141,292.1283)	(141, 292.0622)
(142,292)	(142,292.1283)	(142, 292.0622)
Mean error	0, 0.1283	0, 0.0622

Table 4 Vertical edge sub-pixel coordinates detection

Edge point	Ghosal	Improved algorithm
(316,103)	(316.1284,102.9988)	(315.9375,103.0011)
(316,104)	(316.1301,103.9993)	(315.9381,104.0005)
(316,105)	(316.1270,105.0000)	(315.9407,104.9997)
(316,106)	(316.1267,106.0001)	(315.9389,105.9999)
(316,107)	(316.1250,107.0002)	(315.9404,106.9997)
(316,108)	(316.1259,108)	(315.9381,108.0001)
(316,109)	(316.1259,109)	(315.9386,109)
(316,110)	(316.1259,110)	(315.9385,110)
Mean error	0.1269, 0.0003	0.0611, 0.0003

Table 5 Round edge sub-pixel coordinates detection

Edge point	Ghosal	Improved algorithm
(167,49)	(167.1143,49.1128)	(166.9362,48.9425)
(168,50)	(168.1172,50.1177)	(167.9443,49.9427)
(169,51)	(169.1100,51.1108)	(168.9519,50.9506)
(170,52)	(170.1154,52.1154)	(169.9450,51.9470)
(171,53)	(171.1151,53.1155)	(170.9388,52.9339)
(172,54)	(172.1001,54.0979)	(171.9312,53.9208)
(173,55)	(173.1017,55.0905)	(172.9516,54.9625)
(174,56)	(174.1330,56.1071)	(173.9483,55.9795)
Mean error	0.1133, 0.1085	0.0566, 0.0526

The second experiment is to validate the positioning accuracy of the edge intersections. The test image is a lattice shape image, as shown in Fig. 8. The image has been processed by the edge smoothing to simulate the actual image. The detection results are listed in Table 6. The detection results of the intersections are from the first row to the sixth, and the detection results of the points near an intersection are from the seventh row to the eighteenth. From the detection results, the positioning accuracy of the improved method is much higher than that of Ghosal method.

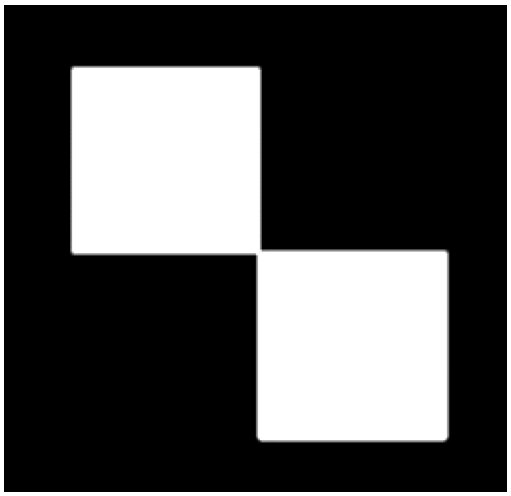

Fig. 8 Lattice shape image

Table 6 Sub-pixel coordinates detection

Edge point	Ghosal	Improved algorithm
(87,45)	(86.6337,45.3721)	(86.9848,45.0159)
(186,45)	(186.3663,45.3721)	(185.9848,44.9841)
(87,144)	(86.6246,143.6124)	(86.9852,143.9843)
(284,142)	(284.3842,142.3796)	(283.9878,141.9879)
(284,242)	(284.5435,241.4888)	(284.0035,242.0146)
(184,242)	(183.4422,241.4857)	(184.0097,241.9932)
(87,46)	(86.6304,46.3390)	(86.9895,46.0168)
(88,45)	(87.6640,45.3100)	(87.9888,45.0195)
(185,45)	(185.3540,45.3100)	(184.9858,44.9837)
(186,46)	(186.3696,46.3390)	(185.9895,45.9832)
(87,143)	(86.6124,142.6493)	(86.9835,142.9871)
(88,144)	(87.6483,143.6056)	(87.9825,143.9886)
(284,143)	(284.3994,143.3553)	(283.9810,142.9855)
(283,142)	(283.3594,142.3046)	(282.9850,141.9843)
(283,242)	(283.3444,241.6554)	(282.9870,242.0198)
(284,241)	(284.3813,240.6538)	(283.9879,241.0148)
(184,241)	(183.6260,240.6572)	(183.9882,240.9844)
(185,242)	(184.6542,241.6564)	(184.9871,241.9852)
Mean error	0.3870, 0.3676	0.0130, 0.0150

In the third experiment, we take TQFP48-P-0707-0.5-K-type chip component as the research object. Figure 9 shows the results of Harris corner feature extractions of the improved method. The detection results of the deflection are listed in Table 2, in which θ is the theoretical deflection angle, θ_1 is the deflection angle detected with pixel Harris corners, θ_2 is the deflection angle detected with sub-pixel Harris-Ghosal method, and θ_3 is the deflection angle detected with the

improved method. The detection results of the offset are listed in Table 3, in which S is the theoretical offset, S_1 is the offset detected with pixel Harris corners, S_2 is the offset detected with sub-pixel Harris-Ghosal method, and S_3 is the offset detected with the improved method. From the detection results, the positioning errors of Harris method are less than 0.1° and 1 pixel, the positioning errors of Ghosal method are less than 0.1° and 0.4 pixels, and the positioning errors of the improved algorithm are less than 0.04° and 0.02 pixels, so the positioning accuracy of the improved algorithm is much higher than that of Hose of Harris or Harris-Ghosal algorithm.

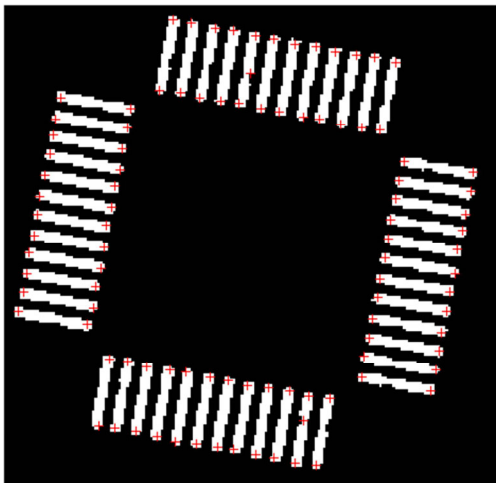

Fig. 9 Results of corner feature extraction

In order to verify the algorithm stability, we analyze the detection results of the improved algorithm in Tables 2 to 8, and the results are listed in Table 9, where "Min" is the minimum of the positioning error's absolute, "Max" is the maximum of the positioning error's absolute, "Mean" is the average value of the positioning error's absolute, and "Std" is the standard deviation of the positioning error's absolute. From the analysis results, the improved algorithm shows good robustness.

Table 7 Detection results of deflection (unit: (°))

θ	θ_1	Error 1	θ_2	Error 2	θ_3	Error 3
1	1.0463	0.0463	1.0425	0.0425	1.0221	0.0221
2	1.9449	0.0551	1.9346	0.0654	1.9760	0.0240
3	2.9634	0.0366	3.0430	0.0430	2.9888	0.0112
4	3.9543	0.0457	3.9450	0.0550	3.9801	0.0199
5	4.9295	0.0705	4.9059	0.0941	4.9666	0.0334
6	6.0744	0.0744	6.0534	0.0534	6.0310	0.0310
7	7.0692	0.0692	7.0547	0.0547	7.0282	0.0282
8	8.0902	0.0902	8.0583	0.0583	8.0338	0.0338
9	9.0491	0.0491	8.9384	0.0616	8.9752	0.0248
10	9.9560	0.0440	9.9589	0.0411	9.9760	0.0240

Table 8 Detection results of offset (unit: pixel)

S	S_1	Error 1	S_2	Error 2	S_3	Error 3
0.5	0	0.5	0.8390	0.3390	0.5152	0.0152
0.6	0	0.6	0.9663	0.3663	0.6159	0.0159
0.7	0	0.7	1.0876	0.3876	0.7148	0.0148
0.8	0	0.8	1.1796	0.3796	0.8157	0.0157
0.9	0	0.9	1.2721	0.3721	0.9122	0.0122
0.99	0	0.99	1.3654	0.3754	1.0046	0.0146
1	1	0	1.3696	0.3696	1.0121	0.0121
1.1	1	0.1	1.4360	0.3360	1.1130	0.0130
1.3	1	0.3	1.6540	0.3540	1.3165	0.0165
1.49	1	0.49	1.8596	0.3696	1.5068	0.0168
1.5	1	0.5	1.8507	0.3507	1.5150	0.0150

Table 9 Stability analysis results

Table No.	Min	Max
2	0.0216, 0.0204	0.0230, 0.0332
3	0, 0.0622	0, 0.0622
4	0.0593, 0	0.0625, 0.0011
5	0.0481, 0.0205	0.0688, 0.0792
6	0.0035, 0.0068	0.0190, 0.0198
7	0.0112	0.0338
8	0.0121	0.0168
Table No.	Mean	Std
2	0.0224, 0.0233	0.0004, 0.0041
3	0, 0.0622	0, 0
4	0.0611, 0.0003	0.0011, 0.0004
5	0.0566, 0.0526	0.0075, 0.0177
6	0.0130, 0.0150	0.0035, 0.0029
7	0.0252	0.0068
8	0.0147	0.0016

9 Conclusions

1) Based on the analysis and comparison to the existing positioning methods of chip components, a new visual positioning method based on Harris corners and Zernike moments is proposed to detect the deflection angle and the offset.

2) For the limitations of Ghosal algorithm, an improved algorithm is presented, in which coarse edge detection method reduced the run time of the next steps.

3) Two formulas are developed to determine the edge intersections, and bilinear interpolation and conjugate gradient method are used to calculate the sub-pixel coordinates of the edge intersections.

4) From the experimental results, it is found that the improved algorithm can simultaneously detect the deflection and the offset shows good positioning effects.

References

[1] LIN C S, LUE L W. An image system for fast positioning and accuracy inspection of ball grid array boards [J]. Microelectronics Reliability, 2001, 41(1): 119−128.

[2] SHANG H L, MING F. A hybrid image alignment system for fast and precise pattern localization [J]. Real-Time Imaging, 2002, 8(1): 23−33.

[3] YEH C H, SHEN T C, WU F C. A case study: Passive component inspection using a 1D wavelet transform [J]. International Journal of Advanced Manufacturing Technology, 2003, 22(11/12): 899−910.

[4] XIE Yang-min, LIU Qiang. Research on locating algorithm of vision alignment system in automatic high precision chip mounter [J]. Optical Technique, 2008, 34(3): 449−454. (in Chinese)

[5] ZHANG Wu-jie, LI Di, YE Feng. Vision-based inspection algorithm for chip components [J]. Journal of South China University of Technology: Natural Science Edition, 2010, 38(1): 65−69. (in Chinese)

[6] LYVERS E P, MITCHELL O R, AKEY M L, REEVES A P. Subpixel measurements using a moment-based edge operator [J]. IEEE Transactions on Pattern Analysis and Machine Intelligence, 1989, 11(12): 1293−1308.

[7] GHOSAL S, MEHROTRA R. Orthogonal moment operators for subpixel edge detection [J]. Pattern Recognition, 1993, 26(2): 295−306.

[8] GAO Shi-yi, ZHAO Ming-yang, ZHANG Lei, ZOU Yuan-yuan. Improved algorithm about subpixel edge detection of image based on Zernike orthogonal moments [J]. Acta Automatica Sinica, 2008, 34(9): 1163−1168. (in Chinese)

[9] GUAN Bai-qing, YU Xin-rui, WANG Shi-gang. An inspection method of component type based on moment features and chain code [J]. Journal of Shanghai Jiao Tong University, 2005, 39(6): 969−974. (in Chinese)

[10] HE Li-feng, CHAO Yu-yan, SUZUKI K, WU Ke-sheng. Fast connected-component labeling [J] Pattern Recognition, 2009, 42(9): 1977−1987.

[11] PAN Yi-feng, HOU Xin-wen, LIU Cheng-lin. A hybrid approach to detect and localize texts in natural scene images [J]. IEEE Transactions on Image Processing, 2011, 20(3): 800−813.

[12] WU Ke-sheng, OTOO E, SUZUKI K. Optimizing two-pass connected-component labeling algorithms [J]. Pattern Analysis and Applications, 2009, 12(2): 117−135.

[13] HSIAO P Y, LU C L, FU L C. Multilayered image processing for multiscale Harris corner detection in digital realization [J]. IEEE Transactions on Industrial Electronics, 2010, 57(5): 1799−1805.

[14] GUEGUEN L, PESARESI M. Multiscale Harris corner detector based on differential morphological decomposition [J]. Pattern Recognition Letters, 2011, 32(14): 1714−1719.

[15] CHEN Zen, SUN Shu-kuo. A Zernike moment phase-based descriptor for local image representation and matching [J]. IEEE Transactions on Image Processing, 2010, 19(1): 205−219.

[16] DA Fei-peng, ZHANG Hu. Sub-pixel edge detection based on an improved moment [J]. Image and Vision Computing, 2010, 28(12): 1645−1658.

[17] CUI J W, TAN J B, ZHOU Y, ZHANG H. Improvement of vision measurement accuracy using Zernike moment based edge location error compensation model [C]// Journal of Physics: Conference Series Harbin, China: IOP Publishing, 2007: 1353−1360.

[18] HAGER W W, ZHANG Hong-chao. A new conjugate gradient method with guaranteed descent and an efficient line search [J]. SIAM Journal on Optimization, 2005, 16(1): 170−192.

[19] YUAN Gong-lin, LU Xi-wen, WEI Zeng-xin. A conjugate gradient method with descent direction for unconstrained optimization [J]. Journal of Computational and Applied Mathematics, 2009, 233(2): 519−530.

[20] PEI Yi-jian, WU Hao, YU Jiang, CAI Guang-hui. Effective image registration based on improved Harris corner detection [C]// International Conference on Information Networking and Automation Kunming, China: IEEE, 2010: 93−96.

[21] MANUEL G S, THURMAN S T, FIENUP J R. Efficient subpixel image registration algorithms [J]. Optics Letters, 2008, 33(2): 156−158.

[22] WYAWAHARE M V, PATIL P M, ABHYANKAR H K. Image registration techniques: An overview [J]. International Journal of Signal Processing, 2009, 2(3): 11−26.

[23] WEN Gong-jian, LU Jin-jian, WANG Ji-yang. An automated method for feature-based image registration with high-accuracy [J]. Journal of Software, 2008, 19(9): 2293−2301. (in Chinese)

[24] LI Qiao-liang, WANG Guo-you, LIU Jian-guo, CHEN Shao-bo. Robust scale-invariant feature matching for remote sensing image registration [J]. IEEE Geoscience and Remote Sensing Letters, 2009, 6(2): 287−291.

[25] GHOSAL S, MEHROTRA R. Detection of composite edges [J]. IEEE Transactions on Image Processing, 1994, 3(1): 14−25.

(Edited by DENG Lü-xiang)